Electromagnetic Simulations of the Partially Coherent Optical Behaviour of Resistive Film TES Detectors

Christopher N. Thomas*† and Stafford Withington*
*Detector and Optical Physics Group, Cavendish Laboratory, JJ Thompson Avenue, Cambridge, CB3 0HE
†Contact: c.thomas@mrao.cam.ac.uk

***Abstract*— Resistive films are a commonly used absorber for free-space coupled TES detectors at sub-mm and far-infrared wavelengths. A formalism is presented for calculating the full partially coherent optical behaviour of such devices in a rigorous way. The scheme is based on a boundary condition on the resistive film, which takes into account the film's finite surface impedance and allows the incident field to be written in terms of the induced current. A Method-of-Moments-like (MoM) approach is then used to invert this relation to give the current in terms of the applied field. Rather then use a set of 'testing functions' as in traditional MoM approaches, a set of dual basis functions is used, leading to a particularly elegant formulation. Using the equation for ohmic power dissipation, it can then be shown the power absorbed by the detector is given by the total contraction of the coherence dyadic of the incident field with a second dyadic field, which will be referred to as the Detector Response Function (DRF). The DRF completely describes the optical behaviour of the detector. The scheme is easily applied to the modelling of arrays of films, allowing cross-talk between pixels to be investigated. We will discuss the details of our method, and present results for the intensity and polarisation response of resistive film TESs to plane wave radiation. In particular, we will concentrate on how the film's dimensions and surface impedance affect its behaviour.**

I. Introduction

A common architecture for free-space-coupled THz detectors is the Transition Edge Sensor (TES), which comprises of a rectangular resistive film and superconducting bilayer on a micro-machined Si_3N_X island. In operation, the bilayer is biased on its normal-superconducting transition and the island's temperature is kept constant by the resulting electro-thermal feedback. Incident radiation induces currents on the film, which dissipate power. The amount of power dissipated can then be measured from the changes in bilayer current needed to maintain island temperature, and this provides a measure of the power flux in the incident radiation.

To fully understand the optical behaviour of such devices, it is vital to understand the relationship between the incident electromagnetic field and the surface currents. The problem is complicated by the possibility of exciting several different current distributions incoherently on the same film. If this is the case the film will be incoherently sensitive to the power in a particular set of modes, with the responsivity of the device varying between the modes. It can be shown that the partially coherent optical behavior of such multi-moded detectors can be described by a two point dyadic response function [1], which we will call the detector response function (DRF). The detector output is given by the total contraction, over some reference surface, of the DRF with the coherence dyadic of the incident radiation.

We have calculated the DRF for resistive film TES detectors rigorously for the first time using a new scheme described in [2]. The scheme is based on a boundary condition on the film, which takes into account the film's finite surface impedance and allows the incident field to be written in terms of the induced current. A Method-of-Moments-like (MoM) approach is then used to invert this relation to give the current in terms of the applied field, and subsequently this can be used to find the DRF from the equation for ohmic power dissipation. Rather then use a set of 'testing functions' as in MoM approaches, a set of dual basis functions is used, leading to a particularly elegant formulation. The scheme is easily applied to the modelling of arrays of films, allowing cross-talk between pixels to be investigated. We will discuss the details of our method, and present results for the intensity and polarisation response of resistive film TESs to plane wave radiation. In particular, we will concentrate on how the film's dimensions and surface impedance affect its behaviour.

The formalism that will be developed is also relevant for understanding the optical behaviour of Kinetic Inductance Detectors (KIDs). A KID is typically comprised of a superconducting microstrip circuit, which is resonant at microwave frequencies, connected to an optical absorber. The device is engineered so that an incident photon generates excess quasiparticles in the superconducting circuit by breaking Cooper pairs. The excess quasiparticles alter the electrical properties of the circuit, and the incident power flux is determined by probing the corresponding changes in the circuit's resonant behaviour. At sub-mm and far-infrared wavelengths a planar-antenna-like structure is commonly employed as the absorber. Quasiparticles are generated by the power dissipated by lossy currents flowing on the antenna. Instead of being lumped at the feed, the antenna load in these absorbers is, in effect, distributed over the entire structure. Consequently, they cannot be treated as conventional antennas, and full electromagnetic simulations must be used to determine the power absorbed. Antenna structures implemented as patterned thin films can be treated identically to the resistive film absorbers for TESs, and the methods outlined in this paper are directly applicable.

II. BASIC FORMALISM

The full formalism for the simulations has been discussed in detail by Withington[2]. This summary will concentrate on the analysis of a single film. The extension to arrays of films is straightforward, but leads to additional notational complexity. It will be discussed briefly at the end of the section, although interested readers should consult the original paper for the complete analysis[2].

In the derivation that follows the incident field will assumed to be temporally stationary, allowing the power absorbed at different wavelengths to be treated independently. Any vector fields introduced should be assumed to be the analytic signal representation of the particular frequency component of the field being considered. The values for the power dissipated represent the power dissipated *per unit bandwidth* at the radiation frequency. However, as we will only consider narrow band illumination and so they may be treated as the total power absorbed by the film.

A. Determining the induced currents

To determine the power absorbed by the resistive film in the TES, it is first necessary to deduce the currents which the incident field excites upon the thin-film absorber. Consider a thin resistive film occupying the region $\mathcal{S}$ of the plane $z = z_0$. Let $\mathbf{r}_t$ denote a point (x, y) on the film's surface, with the absolute position of the point in space given by $\mathbf{r} = \mathbf{r}_t + z_0\hat{\mathbf{z}}$. For simplicity, we will assume that the surface impedance of the film, in Ω, is given by the scalar function $Z_s(\mathbf{r}_t)$. Directional anisotropies in the surface impedance may be included by elevating $Z_s(\mathbf{r}_t)$ to a dyadic function $\bar{\bar{\mathcal{Z}}}_s(\mathbf{r}_t)$, and non-local behaviour by elevating it to a two point function $\bar{\bar{\mathcal{Z}}}_s(\mathbf{r}_{t1}, \mathbf{r}_{t2})$.

The incident electric field $\mathbf{E}_I$ will excite surface currents on the film, and these currents in turn produce a scattered electric field $\mathbf{E}_S$. The current density associated with the induced currents is off the form

$$\mathbf{J}(\mathbf{r}_t, z) = \mathbf{J}_S(\mathbf{r}_t)\delta(z - z_0), \tag{1}$$

where we shall refer to $\mathbf{J}_S$ as the surface current density. As the currents are confined to flow on the surface of the film, $\mathbf{J}_S$ is tangential to the film surface at all points, and as a surface current density it has units Am^{-1}. Following Senior[3], we assume that over the surface of the film, the total electric field –incident plus scattered– and the surface current density satisfy the relation

$$\Big[\bar{\bar{\mathcal{I}}} - \hat{\mathbf{z}}\hat{\mathbf{z}}\Big]\cdot\Big[\mathbf{E}_I(\mathbf{r}_{t1}, z_0) + \mathbf{E}_S(\mathbf{r}_{t1}, z_0)\Big] = Z_s(\mathbf{r}_{t1})\mathbf{J}_S(\mathbf{r}_{t1}). \tag{2}$$

The dyadic acting on $\mathbf{E}_I$ and $\mathbf{E}_S$ simply picks out the component tangential to the film. (2) is essentially the well-known conductivity equation for the current density applied to surface currents, and is used widely in the electromagnetic-modelling community as a starting boundary condition.

We assume now that in the space containing the film there exists a relationship between $\mathbf{E}_S$ and $\mathbf{J}$ in terms of a Green's dyadic of the form

$$\mathbf{E}_S(\mathbf{r}) = \int d^3\mathbf{r}\ \ \bar{\bar{\mathcal{G}}}(\mathbf{r}_1; \mathbf{r}_2)\cdot\mathbf{J}(\mathbf{r}_2). \tag{3}$$

Substituting (3) and (1) into (2) gives

$$\begin{aligned}\Big[\bar{\bar{\mathcal{I}}} - \hat{\mathbf{z}}\hat{\mathbf{z}}\Big]\cdot\mathbf{E}_I(\mathbf{r}_{t1}, z_0) \ &= Z_S(\mathbf{r}_{t1})\mathbf{J}_S(\mathbf{r}_{t1}) - \\ \Big[\bar{\bar{\mathcal{I}}} - \hat{\mathbf{z}}\hat{\mathbf{z}}\Big]\cdot\int d^2\mathbf{r}_{t2}\ \ \bar{\bar{\mathcal{G}}}(\mathbf{r}_{t1}, z_0; \mathbf{r}_{t2}, z_0)\ \cdot\mathbf{J}_S(\mathbf{r}_{t2}, z_0).\end{aligned} \tag{4}$$

This equation gives the tangential component of the incident field if the surface current is known, and must be inverted to give the current from the incident field. This is done by writing $\mathbf{J}_S$ and $\Big[\bar{\bar{\mathcal{I}}} - \hat{\mathbf{z}}\hat{\mathbf{z}}\Big]\cdot\mathbf{E}_I$ in decomposed form,

$$\mathbf{J}_S(\mathbf{r}_t) = \sum_n \alpha_n \mathbf{U}_n(\mathbf{r}_t) \tag{5}$$

and

$$\Big[\bar{\bar{\mathcal{I}}} - \hat{\mathbf{z}}\hat{\mathbf{z}}\Big]\cdot\mathbf{E}_I(\mathbf{r}_t, z_0) \ = \sum_m \beta_m \mathbf{V}_n(\mathbf{r}_t). \tag{6}$$

The basis functions set used for the field and the current need not been the same, and the sets need not be individually orthogonal. Basis functions can be defined over a sub-region of the film (local) or defined over the entire film (global). Localised basis functions are useful for first determining the surface current distributions that can be excited on a film. For array simulations, where it is beneficial to use small basis sets, they may then be replaced with a reduced set of global basis functions chosen to best span the current distributions observed. Substituting (5) and (6) in (4) yields

$$\begin{aligned}\sum_m \beta_m \mathbf{V}_n(\mathbf{r}_{t1}) = \sum_n \alpha_n\ \Big(&Z_s(\mathbf{r}_{t1})\mathbf{U}_n(\mathbf{r}_{t1}) - \\ &\Big[\bar{\bar{\mathcal{I}}} - \hat{\mathbf{z}}\hat{\mathbf{z}}\Big]\cdot\int d^2\mathbf{r}_{t2}\ \bar{\bar{\mathcal{G}}}(\mathbf{r}_{t1}, z_0; \mathbf{r}_{t2}, z_0)\ \cdot\mathbf{U}_n(\mathbf{r}_{t2})\Big).\end{aligned} \tag{7}$$

In a traditional MoM approach[4], a set of so-called weighting and testing functions would now be introduced. The inner product of these functions with (7) is would then be taken to generate a matrix equation. Instead we will make use of the duals, $\{\tilde{\mathbf{V}}_m(\mathbf{r}_t)\}$, of the field basis functions, $\{\mathbf{V}_m(\mathbf{r}_t)\}$. The dual basis set is defined such that

$$\int d^2\mathbf{r}_t\ \tilde{\mathbf{V}}^*_m(\mathbf{r}_t)\cdot\mathbf{V}_n(\mathbf{r}_t) = \delta_{mn}, \tag{8}$$

and its explicit calculation is discussed in [5]. Left multiplying (7) by the conjugate of each dual basis function, then integrating, results in the matrix equation

$$\boldsymbol{\beta} = \Big(\mathsf{Z} - \mathsf{G}\Big)\cdot\boldsymbol{\alpha}, \tag{9}$$

where

$$\mathsf{Z}_{mn} = \int d^2\mathbf{r}_t\ Z_S(\mathbf{r}_t)\,\tilde{\mathbf{V}}^*_m(\mathbf{r}_t)\ \cdot\mathbf{U}_n(\mathbf{r}_t), \tag{10}$$

and

$$\mathsf{G}_{mn} = \int d^2\mathbf{r}_{t1}\int d^2\mathbf{r}_{t2}\ \tilde{\mathbf{V}}^*_m(\mathbf{r}_{t1})\cdot\bar{\bar{\mathcal{G}}}(\mathbf{r}_{t1}, z_0; \mathbf{r}_{t2}, z_0)\cdot\mathbf{U}_n(\mathbf{r}_{t2}). \tag{11}$$

Relation (2) has successfully been reduced to a matrix equation, and may be inverted by finding the pseudo inverse of the matrix on the left hand side. Letting, $\mathsf{M} = (\mathsf{Z} - \mathsf{G})^{-1}$, we have explicitly that

$$\boldsymbol{\alpha} = \mathsf{M}\cdot\boldsymbol{\beta}. \tag{12}$$

Using (6) and (8) it is straightforward to show that

$$\beta_m = \int d^2\mathbf{r}_t \ \tilde{\mathbf{V}}^*_m(\mathbf{r}_t) \cdot \mathbf{E}_I(\mathbf{r}_t, z), \tag{13}$$

This allows the decomposition coefficients for the incident field to be found, which may then be used with (12) and (5) to construct the induced current. Consequently once M has been found for the particular film, we are able to calculate the current induced on it by any incident field at the relevant wavelength.

B. Determining the power dissipated in the absorbing film

Of principle interest to us is the total power P dissipated in the film, as it is to this that the TES as a whole is sensitive. The power dissipated by the currents is given by

$$P = \frac{1}{2}\int d^2\mathbf{r}_t \ \Re[Z_s(\mathbf{r}_t)]|\mathbf{J}_S(\mathbf{r}_t)|^2. \tag{14}$$

Substituting (5) into (14), we find that the P can be written in terms of the current decomposition coefficients as

$$P = \frac{1}{2}\boldsymbol{\alpha}^\dagger \cdot \mathsf{C} \cdot \boldsymbol{\alpha}, \tag{15}$$

where

$$\mathsf{C}_{mn} = \int d^2\mathbf{r}_t \ \Re[Z_S(\mathbf{r}_t)]\mathbf{U}^*_m(\mathbf{r}_t) \ \cdot \mathbf{U}_n(\mathbf{r}_t). \tag{16}$$

The expression for P in terms of the field decomposition coefficients follows logically using (12):

$$P = \frac{1}{2}\boldsymbol{\beta}^\dagger \cdot \ \mathsf{M}^\dagger \cdot \mathsf{C} \cdot \mathsf{M} \cdot \boldsymbol{\beta}. \tag{17}$$

The power absorbed can now be calculated for a given incident field.

C. The Detector Response Function (DRF)

A very powerful result can be obtained by substituting (13) into (17). Letting

$$\mathsf{D} = \frac{1}{2}\mathsf{M}^\dagger \cdot \mathsf{C} \cdot \mathsf{M}, \tag{18}$$

we obtain

$$\begin{aligned} P = &\sum_m \sum_n \int d^2\mathbf{r}_{t1} \int d^2\mathbf{r}_{t2} \\ &\mathsf{D}_{mn}\Big(\tilde{\mathbf{V}}^*_m(\mathbf{r}_{t2}) \cdot \mathbf{E}_I(\mathbf{r}_{t2}, z)\Big)^* \Big(\tilde{\mathbf{V}}^*_n(\mathbf{r}_{t1}) \cdot \mathbf{E}_I(\mathbf{r}_{t1}, z)\Big). \end{aligned} \tag{19}$$

The kernel of this integral may be written in a more instructive form by adopting double dot notation for dyadics:

$$\begin{aligned} &\sum_m \sum_n \mathsf{D}_{mn}\Big(\tilde{\mathbf{V}}^*_m(\mathbf{r}_{t2}) \cdot \mathbf{E}_I(\mathbf{r}_{t2}, z)\Big)^* \Big(\tilde{\mathbf{V}}^*_n(\mathbf{r}_{t1}) \cdot \mathbf{E}_I(\mathbf{r}_{t1}, z)\Big) \\ &= \Big(\sum_m \sum_n \mathsf{D}_{mn}\tilde{\mathbf{V}}_m(\mathbf{r}_{t2}) \ \tilde{\mathbf{V}}^*_n(\mathbf{r}_{t1})\Big) \cdot\cdot \Big(\mathbf{E}_I(\mathbf{r}_{t1}, z)\mathbf{E}^*_I(\mathbf{r}_{t2}, z)\Big). \end{aligned} \tag{20}$$

Using (20) and then taking the ensemble average of (19) gives

$$< P >= \int d^2\mathbf{r}_{t1} \int d^2\mathbf{r}_{t2} \ \bar{\bar{\mathcal{D}}}^\dagger(\mathbf{r}_{t1}; \mathbf{r}_{t2}) \cdot\cdot \bar{\bar{\mathcal{E}}}(\mathbf{r}_{t1}; \mathbf{r}_{t2}), \tag{21}$$

where

$$\bar{\bar{\mathcal{E}}}(\mathbf{r}_{t1}; \mathbf{r}_{t2}) = \Big\langle \ \mathbf{E}_I(\mathbf{r}_{t1}, z)\mathbf{E}^*_I(\mathbf{r}_{t2}, z)\Big\rangle \tag{22}$$

is the correlation dyadic of the incident field, or EFC, and

$$\bar{\bar{\mathcal{D}}}(\mathbf{r}_{t1}; \mathbf{r}_{t2}) = \sum_m \sum_n \mathsf{D}_{mn} \ \tilde{\mathbf{V}}_m(\mathbf{r}_{t1})\tilde{\mathbf{V}}^*_n(\mathbf{r}_{t2}). \tag{23}$$

is the Detector Response Function, or DRF.

Equation (21) completely describes the optical response of the detector to partially coherent fields[1], [6]. The relationship between the DRF and the detector is analogous to that between an antenna and its reception pattern. However, whereas the reception pattern of a classical antenna is a fully coherent field, the DRF is a partially coherent field. It describes the state of coherence of the incident field in which the detector is sensitive to power. The amount of power absorbed by the detector depends on how well the actual state of coherence of the field, described by the ECF, 'overlaps' with the desired state. (21) is simply the inner product between these two state vectors in an abstract space. Like a reception pattern, the DRF can be back-propagated through an optical system to determine the responsivity of the detector to power on a different reference surface. As a partially coherent field, the DRF admits a decomposition in terms of coherent modes. These coherent modes, which are called the natural modes of the detector, correspond to the modes of incident field in which the detector is incoherently sensitive to power.

D. Extension to arrays of films

For an array of films, the boundary condition (2) must be satisfied on each film. Again the incident field and surface current density on each film are in expanded in a set of basis functions. A matrix equation is set up as in section II-A, remembering to take into account the cross terms between basis functions on different films (which are coupled by $\bar{\bar{\mathcal{G}}}(\mathbf{r}_{t1}, \mathbf{r}_{t2})$). The process of finding the induced currents then follows in the same way as in the case of the single film. When calculating the power absorbed, the currents over a sub-set of films - ranging from an individual pixel to an array sub-cell - can be considered and the appropriate DRF for that sub-assembly found. This formulation takes into full account the electromagnetic cross talk between members of the array when considering the behaviour of single elements.

III. Simulation details

A. Arrangement considered

As a first application of the scheme outlined above, we have studied the optical properties of square films in free space as a function of the film size and surface impedance. The simulations represent the behaviour expected for a single resistive film TES bolometer isolated from any scattering structure. This is an unlikely configuration in reality, as such devices are typically employed in imaging arrays where, at minimum, there will be scattering from adjacent pixels. Simulations of full arrays are computationally intensive, and it is desirable for efficiency to use the smallest possible basis set on each film that can adequately describe the current distributions that

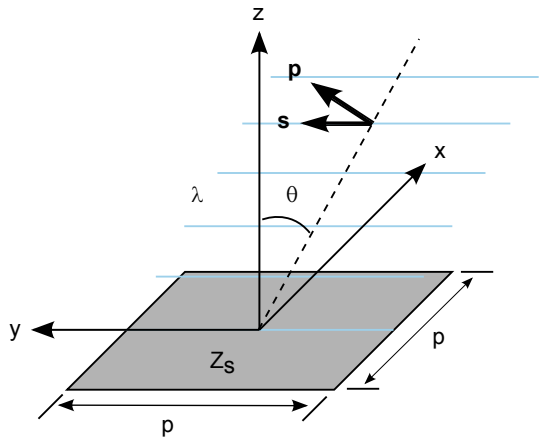

Fig. 1. Diagram showing the arrangement considered in the simulations and the notation used for the incident radiation.

may be excited. Simulations on a single detector are useful for determining these current distributions, and are therefore an important first step in the analysis of a full array. In addition, in a recent paper [7] we have proposed a simplified model for the electromagnetic behaviour of thin-film absorbers and investigated the resulting optical behaviour. Part of our motivation for performing simulations on single detectors was for comparison with this previous work. In particular, we were keen to determine the exact conditions under which the model is a good approximation to the actual behaviour. Finally, we are also interested in how the optical behaviour of the detector may be altered by patterning the absorbing film. This is best investigated initially without the additional complication of scattering from other structures.

Figure 1 illustrates the geometry considered. The film is assumed to a square of side length p lying at the centre of the plane $z = 0$. In subsequent sections we consider illuminating the film with a monochromatic plane wave of wavelength λ, and it is useful to consider the form the incident field takes. We restrict ourselves to waves whose direction of incidence is in the (x, z) plane, and will use θ to denote the angle the direction of travel makes with the positive z-direction. The functional form of the incident field over the film's surface is given by

$$\mathbf{E}(\mathbf{r}_t) = E_0 \exp[-ikx\sin\theta] \begin{cases} \cos\theta\hat{\mathbf{x}} - \sin\theta\hat{\mathbf{z}} & \text{p-polarised} \\ \hat{\mathbf{y}} & \text{s-polarised,} \end{cases} \tag{24}$$

where $k = 2\pi/\lambda$ and we adopted the normal p and s polarisation states. In the sections that follow we will concentrate on the optical behaviour of the film under these illumination conditions.

B. Implementation details

The film is assumed to be in free space, so the Green's dyadic $\bar{\bar{\mathcal{G}}}(\mathbf{r}_{t1}, z_1; \mathbf{r}_{t2}, z_2)$ for the problem is

$$\bar{\bar{\mathcal{G}}}(\mathbf{r}_{t1}, z_1; \mathbf{r}_{t2}, z_2) = i\omega\mu_0 \Big(\bar{\bar{\mathcal{I}}} + \frac{1}{k^2}\nabla_1\nabla_1 \Big)\, g(\mathbf{r}_{t1}, z_1; \mathbf{r}_{t2}, z_2), \tag{25}$$

with

$$g(\mathbf{r}_{t1}, z_1; \mathbf{r}_{t2}, z_2) = \frac{\exp\left[ik\sqrt{|\mathbf{r}_{t1} - \mathbf{r}_{t2}|^2 + (z_1 - z_2)^2}\right]}{4\pi\sqrt{|\mathbf{r}_{t1} - \mathbf{r}_{t2}|^2 + (z_1 - z_2)^2}}. \tag{26}$$

It is immediately obvious that the Green's dyadic is singular when both $\mathbf{r}_{t1} = \mathbf{r}_{t2}$ and $z_1 = z_2$, and that this complicates the numerical evaluation of the integrals in (11). We are free to choose to the current basis functions and field dual functions, and by careful choice we can to some extent alleviate these numerical problems. In our simulations we employed the same set of Rao, Wilson and Glisson (RWG) basis functions[8] defined on a square mesh for both sets for both functions. RWG basis functions are used extensively in the MoM community, and the evaluation the integral of their product with the free space Green's dyadic is well documented. The approach taken is to break the kernel of the integrals up into a singular and non-singular part, a procedure called extracting the singularity. The non-singular part is then handled numerically, whilst the singular part when RWG basis functions are used is simple enough that it may be evaluated analytically[9]. Using the same set of basis functions for the current basis and field duals also has the advantage $\mathsf{Z} = \mathsf{C}$, reducing the computations that must be performed.

C. Simple model for the excited current

Full electromagnetic simulations may be to cumbersome for some design problems. In these circumstances it is useful to have a simpler model for the film's behaviour, and to know the regimes in which its use is valid. As a first approximation to the full behaviour, the non-local response introduced by the scattered field can be ignored. The surfaced current, $\mathbf{J}_S(\mathbf{r}_t)$, induced at a point on the film then depends only on the incident field, $\mathbf{E}_I(\mathbf{r}_t)$, at that point. Naively, we might then assume that $\mathbf{J}_S(\mathbf{r}_t) \approx \mathbf{E}_I(\mathbf{r}_t)/Z_S(\mathbf{r}_t)$ will be a good model for the induced currents. However, it is unphysical as in the limit $Z_S \to 0$ the surface current density tends to infinity at all points.

For guidance we consider the analytically soluble problem of a plane wave incident normally on an infinite film. From the translational invariance of the problem, the wave must excite an infinite sheet current. It can be shown that the electric field radiated by an infinite current sheet lying in the plane $z = 0$ is given by

$$\mathbf{E}_S(z) = -\frac{Z_0}{2}\mathbf{J}_S \exp(ik|z|), \tag{27}$$

where Z_0 is the impedance of free space. Using (27) in (2) and rearranging gives

$$|\mathbf{J}_S| = \frac{|\mathbf{E_I}|}{Z_s + \frac{1}{2}Z_0}, \tag{28}$$

where the effect of scattering appears to be to increase the effective surface impedance seen on induction by $\frac{1}{2}Z_0$. Adopting this effective surface impedance as the proportionality constant, we have for our simple model

$$\mathbf{J}_S(\mathbf{r}_t) \approx \frac{1}{Z_S + \frac{1}{2}Z_0} \left(\bar{\bar{\mathcal{I}}} - \hat{\mathbf{z}}\hat{\mathbf{z}}\right)\cdot\mathbf{E}_I(\mathbf{r}_t, z_0), \tag{29}$$

where the dyadic operator is there so the induced current only has components tangential to the surface. In the subsequent sections we shall compare this model with the simulation results to determine the limits of its application. The optical behaviour associated with this simple model is investigated in detail in [7].

IV. Simulation results

A. Current distributions excited by an s-polarised plane wave

In order to understand power absorption by the film, it is useful to first consider the spatial form of the induced currents. Figure 2 shows the current distribution induced on films of various size and surface impedance by an s-polarised plane wave incident from $\theta = 0°$. Film size, p/λ, increases across the rows of the figure, and the surface impedance of the film, Z_s down the its columns. In each plot the black line shows the current along the cut $(x, 0, 0)$, and the grey line the currents along the cut $(0, y, 0)$. For both cuts the magnitude of the dominant component J_y of the surface current is plotted, and it is normalised to the incident magnetic field intensity H to remove the dependence on incident field strength. For all the simulations, a 41×41 sub-domain mesh was used and convergence of the solution was checked. Where the approximate model (29) is valid, we expect the plots in fig. 2 to be straight lines at

$$\frac{|J_y|}{|H|} \approx \frac{2Z_0}{2Z_S + Z_0}. \tag{30}$$

The current distributions found for perfectly electrically conducting (PEC) films (top row of figure 2) are in agreement with those in the literature[8], providing validation of the code. Across the rows of figure 2, where $\frac{p}{\lambda}$ is increasing, the surface current distribution along both cuts are observed globally to flatten out. Flatten here is used to mean that the scale of any variation in $|J_y|$ decreases relative to the mean value. On local scales we see the development of standing wave like patterns in $|J_y|$, and these most likely result from the trapping of the scattered field between film edges. For fixed Z_S, as $\frac{p}{\lambda}$ is increased the mean current level is observed to remain approximately constant. However, this should not be taken as meaning the power absorbed will scale simply with the increased area. Remember that the local power dissipation scales with $|J_y|^2$, making P sensitive to the precise spatial current distribution. By the same principle, we see that in electrically small, low Z_S films, the edges are the regions of highest power dissipation. Down the columns of figure 2, where Z_S is increasing, the same flattening of the current distributions is observed. However, there is no accompanying development of fine scale structure and, for fixed $\frac{p}{\lambda}$, as Z_S is increased the mean current along each cut decreases.

Visually, the current distributions obtained agree best with the predictions of (29) when either $\frac{p}{\lambda}$ is larger than unity and/or Z_S is large compared with Z_0. The numerical values for the current in these regimes are also in good agreement with the values expected from (30), which have been collated in table I. When Z_s is large, Z dominates the right-hand-side of (9). For a uniform impedance film we then have $\mathsf{M} \approx Z_S\mathsf{I}$, or $\mathbf{J}_S(\mathbf{r}_t) \approx \mathbf{E}_I(\mathbf{r}_t)/Z_S$. This is the same as (29) when $Z_S >> Z_0$. Physically, when Z_S is high the induced currents are small so the scattered field is weak and can be ignored – this is the main assumption made in the simple model. When $\frac{p}{\lambda}$ is large, the edges only weakly effect the behaviour in the bulk of the film and it may essentially treated as being infinite in dimension. Since we used the case of an infinite film to guide our model, it is expected they will agree.

$\lvert J_y\rvert/\lvert H_x\rvert$	Z_S/Z_0
0.00	2.00
0.50	1.00
1.00	0.67
2.00	0.40
10.0	0.10

TABLE I
VALUES OF $|J_y|/|H_x|$ AS A FUNCTION Z_S PREDICTED BY SIMPLE MODEL

Figure 3 is the equivalent of figure 2 for a plane wave incident at angle $\theta = 90°$, i.e. edge-on. The current distribution along the $(0, y, 0)$ cut is, in all cases, similar in shape to that observed for a normally incident wave. Along the $(0, x, 0)$ cut different behaviour is observed. When Z_S is less than Z_0, in general the current distribution along $(0, x, 0)$ is peaked at the leading edge of the film, then decays exponentially in the direction of propagation of the wave across the film. This is the effect is a result of the currents on leading edge screening the bulk film. It means that for large, low Z_S, films the majority of the induced current is confined to a small strip near the edge when $\theta = 90°$. This fact will become important in the next section when we discuss how the edge on absorption cross section scales with p.

Similar trends in the current distributions excited by the edge-incident wave are observed for increasing $\frac{p}{\lambda}$ and Z_S as for the normally-incident wave. One difference is that with Z_S fixed, the mean current now decreases as $\frac{p}{\lambda}$ increases due to the decay over the films surface. In the limit $\frac{p}{\lambda} > 1$ and $Z_S > Z_0$ the simulations for the edge incident wave are still in good numerical agreement with the simple model, even though it was formulated assuming a normally incident wave.

It is worth noting that since currents are excited on the film when an s-polarised wave is incident edge-on, power is dissipated and the TES is therefore be sensitive to radiation incident from edge-on. This is a fact which may not be immediately obvious, and is discussed in detail in the next sub-section. It has important implications for the stray-light sensitivity of thin film devices.

B. Effective area of the film as a function of θ and the polarisation

A useful measure of the ability of a film to extract power from the incident plane wave is the effective area, A_E. The effective area is ratio of the total power P dissipated in the film to the power flux in the incident wave:

$$A_E = \frac{2Z_0 P}{|E_0|^2}. \tag{31}$$

Obviously, A_E will be a function of both the direction of incidence and polarisation of the plane wave. Usually we plot

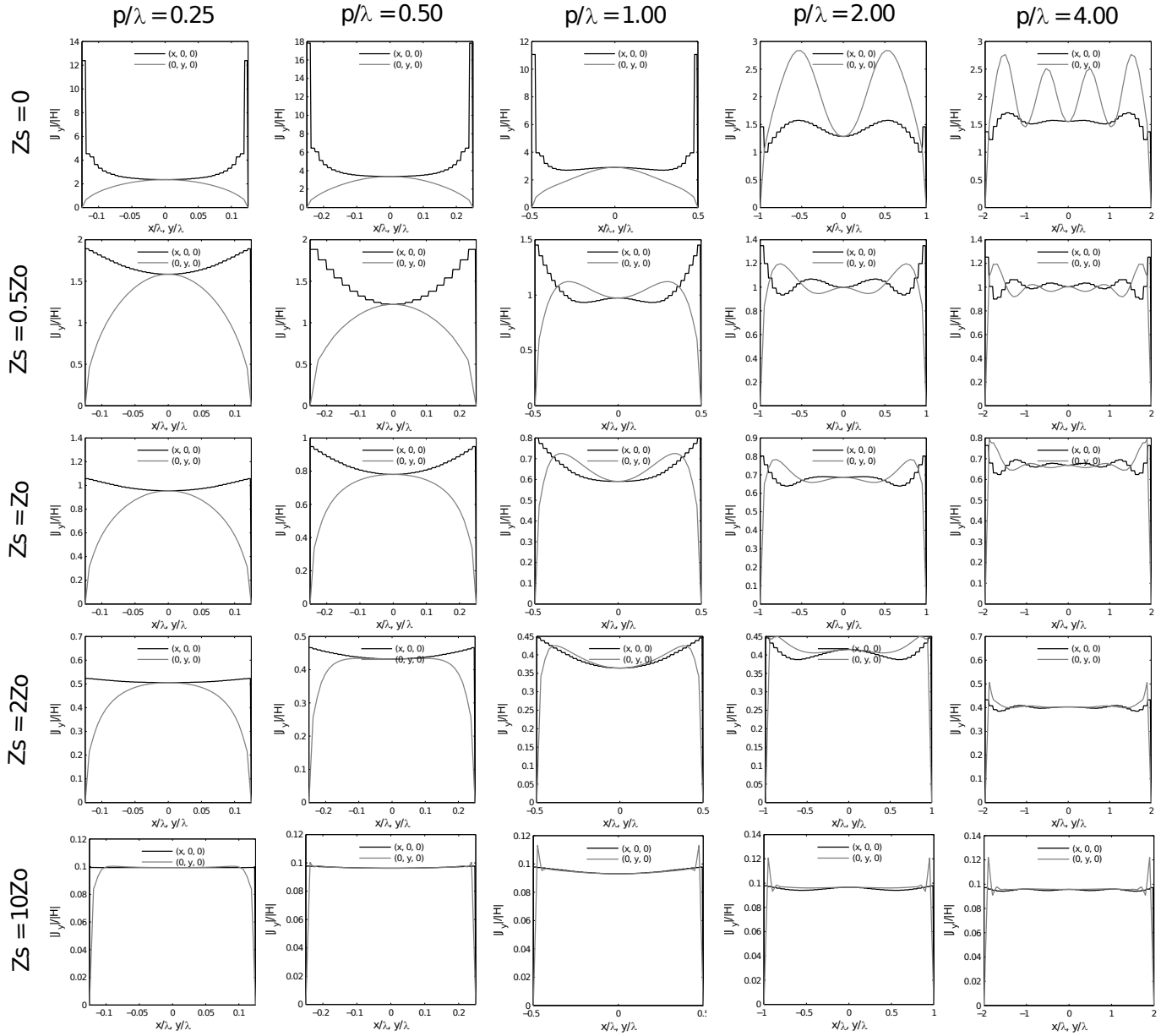

Fig. 2. Plots showing the current distributions excited by an s-polarised wave incident at an angle $\theta = 0°$.

A_E/λ^2 and use $\frac{p}{\lambda}$, as this allows the scaling of the results from the simulation to any physical scale.

We will restrict ourselves to plane waves incident according to the restrictions in III-A. With the approximate model of the induced current, using (29), (14) and (24) gives

$$\frac{A_E(\theta)}{\lambda^2} = \frac{4Z_0 Z_S}{(2Z_S + Z_0)^2}\left(\frac{p}{\lambda}\right)^2 \begin{cases} 1 & \text{s-polarised} \\ \cos^2\theta & \text{p-polarised.} \end{cases} \quad (32)$$

Notice that the response to s-polarised waves is expected to be isotropic in the regime where the model is valid, i.e. the film should be as sensitive to plane waves incident edge on as it is face on. It may at first appear surprising that the film is sensitive to power incident edge-on, but remember that the **E**-field when the wave is s-polarised and $\theta = 90°$ is directed tangential to the film surface. It is, therefore, still able to excite a surface current and dissipate power. By contrast the **E**-field associated with the equivalent p-polarised wave is normal to film, is unable to force a current and so $A_E(90°) = 0$. The normal and edge-on cross sections for p-polarised radiation are the same in the simple model as the currents excited by the two waves are identical. This is not the case in reality, as will be seen shortly.

Figure 4 shows polar plots of A_E as a function of θ and polarisation direction for films of several different values of $\frac{p}{\lambda}$ and Z_S. The size of film decreases down the rows of the array, and the surface impedance Z_S increases across the columns. These plots describe the angular response that would be expected from a resistive film bolometer.

At low Z_S the results for the $4\lambda \times 4\lambda$ film (first row of figure 4) are as we might have expected intuitively. $A_E(0°)$ for both the p- and s-polarised wave is approximately half the physical pixel area (except at very low Z_S). For the s-polarised

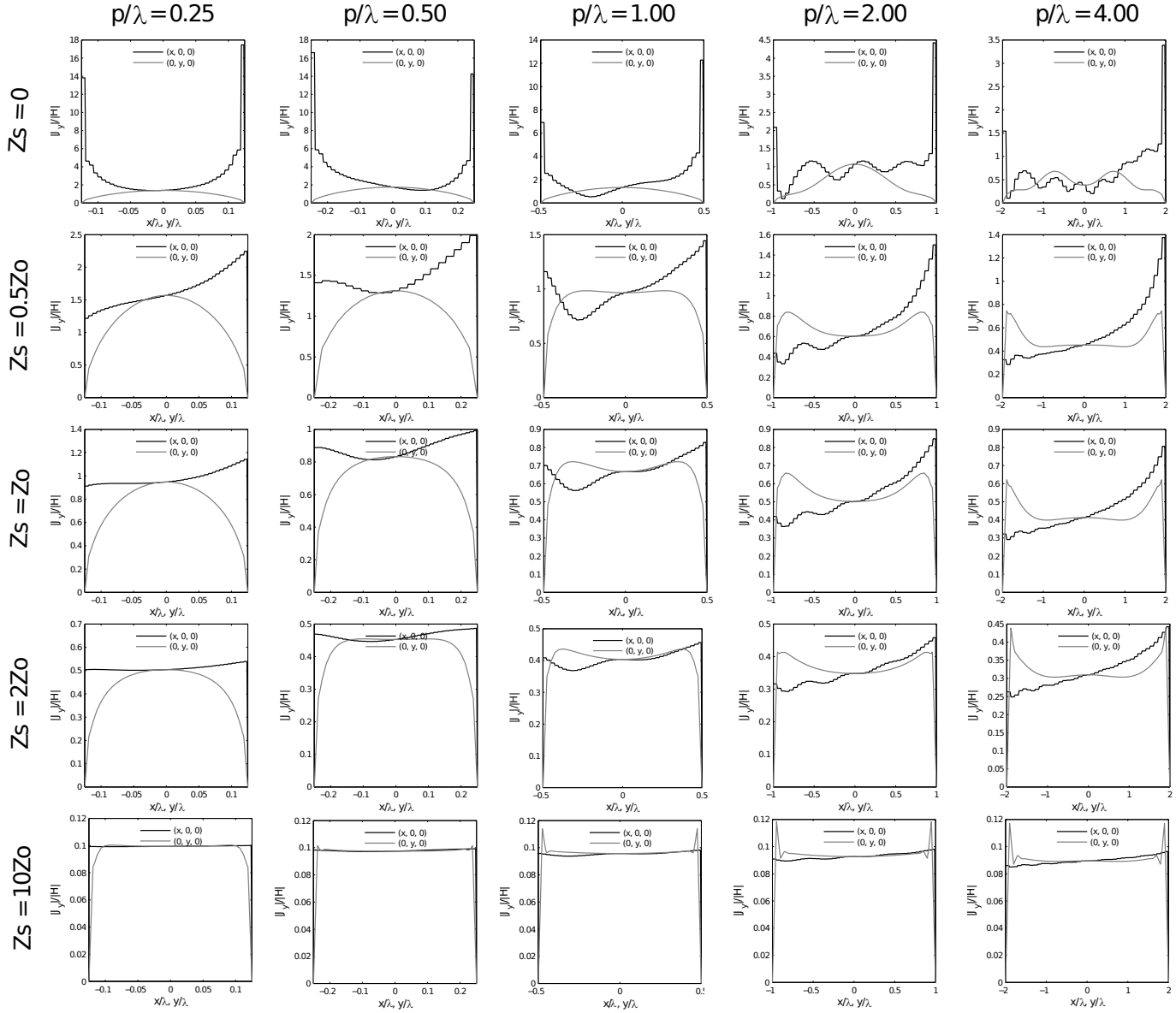

Fig. 3. Plots showing the current distributions excited by an s-polarised wave incident at an angle $\theta = 90^\circ$.

wave, $A_E(90^\circ)$ is zero for the reasons explained above. For the p-polarised wave $A_E(90^\circ)$ is finite, but still much smaller than the face-on cross section. Generally, for the p-polarised plane the film behaves as it is comprised of two Lambertian absorbers, one of which is orientated parallel to the film and the other normal to it. As Z_S is increased the response to the s-polarised wave becomes more forward directed, while $A_E(90^\circ)$ is seen to increase towards $A_E(0^\circ)$. At very low Z_S, the films absorption patterns exhibit lobe structure like an antenna.

The A_E curves for the $\lambda \times \lambda$ and $0.25\lambda \times 0.25\lambda$ film (rows two and three of figure 4) have a similar structure to those for the much larger film. However, for all Z_S the values of $A_E(0^\circ)$ and $A_E(90^\circ)$ for the p-polarised wave are more comparable. At low Z_S, $A_E(90^\circ)$ even exceeds $A_E(0^\circ)$, which is not intuitive. At high Z_S, the results for electrically small films are in excellent agreement with the behaviour predicted by (32).

It is worth considering how the effective area for a s-polarised edge-incident wave can exceed that for a normally incident wave of the same polarisation, as observed for the electrically small films in figure 4 when $Z_0 < Z_s$. This behaviour can be explained in terms of the current distributions observed in section IV-A. When an s-polarised plane is normally incident, the induced current can be approximated as a uniform sheet. The magnitude of the current is approximately independent of film size (figure 2), so we expect the total power absorbed, and thus $A_E(0^\circ)$, to scale as p^2. For the equivalent edge incident wave, if $Z_s < Z_0$ the current is confined to a narrow strip at the leading edge of the film. Its value on the leading edge for fixed Z_S is approximately independent of the film size (figure 3), so we expect $A_E(90^\circ)$ to scale as p. This result also follows by noting that the narrow strip current at the edge should behave like a thin-wire antenna. These simple scaling rules can be seen to roughly hold for the

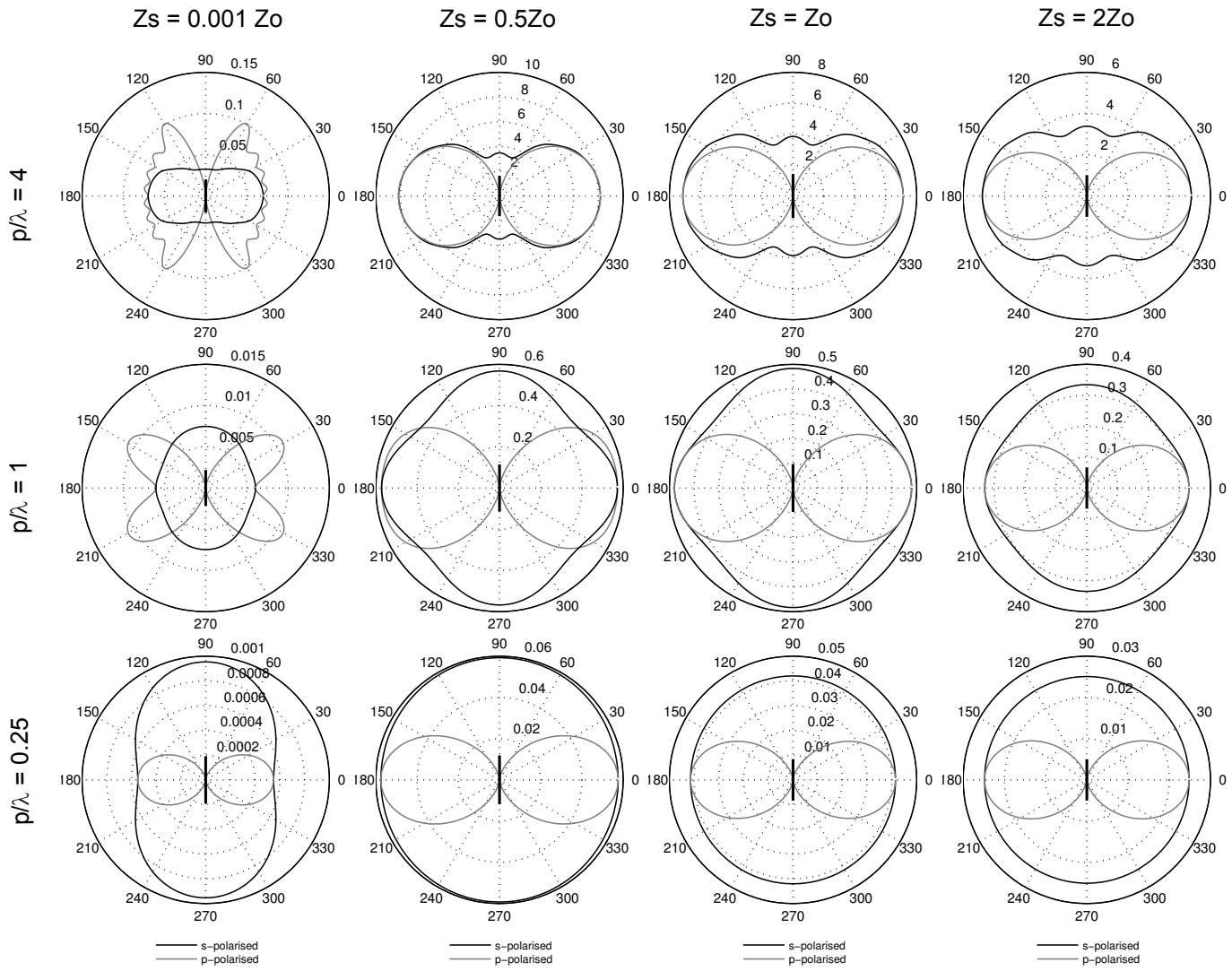

Fig. 4. Plots showing the effective area of the absorber as a function of polarisation and incidence angle. A_E/λ^2 is plotted on the polar axis.

values in table II, which are for a film with $Z_S = 0.5Z_0$. If $A_E(0°) \propto p^2$ and $A_E(90°) \propto p$ hold for all p, it is always possible to find a value of p below which $A_E(90°)$ is greater then $A_E(0°)$. This explains why, when $Z_S < Z_0$, the edge-incident value of A_E for an s-polarised wave exceeds the value for normal incidence only once the film falls below a certain size relative to the wavelength, e.g. figure 4.

Extrapolating in the other direction, for $Z_S < Z_0$ we would expect $A_E(90°)$ to grow much faster with p then $A_E(0°)$ for the p-polarised wave. For large, low impedance films, the A_E for a normal incident wave should therefore greatly exceed A_E for edge-on wave, as observed in the data. When $Z_S > Z_0$, from figure 3 we see that for edge-incident waves the current is less concentrated at the leading edge. In this circumstance, we would therefore expect $A_E(90°) \propto p^2$. This should mean for high Z_S films that $A_E(0°)$ and $A_E(90°)$ should be comparable for all p, in agreement with the observed trends.

Finally it is traditionally assumed that a free-standing thin film is only able to absorb, at maximum, half of the power incident upon it. We would therefore expect A_E to always be less than or equal to half the film's geometric area, p^2.

p/λ	$A_E(\theta = 0°)$	$A_E(\theta = 90°)$
0.25	0.06	0.06
0.50	0.17	0.20
1.00	0.60	0.60
2.00	2.00	1.5
4.00	8.00	3.5

TABLE II
A_E/λ^2 AS A FUNCTION OF p FOR A WAVE INCIDENT NORMALLY AND EDGE-ON, $Z_S = 0.5Z_0$.

This indeed the case when $p > \lambda$ in figure 4, however for the electrically small films values of A_E almost equal to the physical area are observed. It is well known from antenna theory that the effective area of an electrically small antenna can exceed its physical area (e.g. the Hertzian dipole), and the observed behaviour is simply a manifestation of this effect.

C. Detector Response Function (DRF)

The DRF was introduced in section II-C and fully describes the response of the detector to partially coherent radiation. A

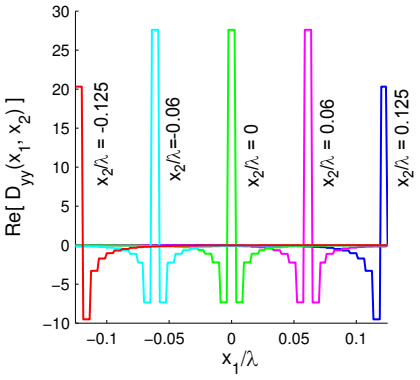

Fig. 5. Plot of part of the DRF for a 188.5Ω $0.25\lambda \times 0.25\lambda$ film. $y_1 = y_2 = 0$

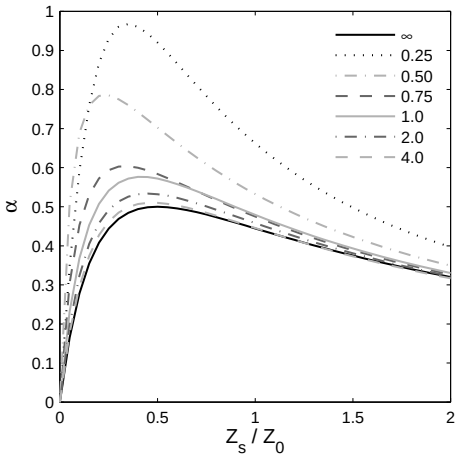

Fig. 6. $\alpha = A_E(\theta = 90°)/p^2$ vs Z_S for various film sizes

useful physical picture of the DRF is as the correlation dyadic, (22), of the particular state of coherence of the incident field to which the detector is responsive. A natural terminology that then arises is to describe the detector response as coherent, partially-coherent or incoherent depending on the level of coherence in the field the DRF describes. As an example, consider the DRF predicted using the simple model for the electromagnetics of the field from III-C. Substituting (29) into (14), it is straightforward to show that

$$\bar{\bar{\mathcal{D}}}(\mathbf{r}_{t1}, \mathbf{r}_{t2}) = \frac{Z_S}{2(Z_S + Z_0/2)^2} \left(\bar{\bar{\mathcal{I}}} - \hat{\mathbf{z}}\hat{\mathbf{z}}\right)\delta(\mathbf{r}_{t1} - \mathbf{r}_{t2}), \quad (33)$$

which represents a fully incoherent response. Power detectors that use traditional antennas, for example a microwave radiometer, are an example of a fully coherent detector. Partially coherent detectors show intermediate behaviour, with the DRF taking non-zero for small values of $|\mathbf{r}_{t1} - \mathbf{r}_{t2}|$.

Space precludes a full discussion of DRFs calculated for the resistive films, but fig. 5 has been included to show the general behaviour. The data in the plot is for a $0.5\lambda \times 0.5\lambda$ film with uniform surface impedance $Z_S = 0.5Z_0$. There are two main problems that arise when trying to represent DRFs graphically. The first is that they function of two position vectors, which in this case results in a four-parameter function $\bar{\bar{\mathcal{D}}}(x_1, y_1; x_2, y_2)$. For all the lines in fig. 5, y_1 and y_2 are zero, while each line represents results for a different value of x_2 (which are equally spaced along the cut $(x, 0, 0)$). This leaves x_1 as the dependent variable. The second difficulty is that the dyadic has multiple elements. In fig 5 only the yy component is shown. A sharp peak in each line is observed at point where $x_1 = x_2$. Further simulations have shown that these peaks behave like delta functions, and correspond to the incoherent part to the film's response. Unlike the behaviour predicted by (33), the incoherent response is non-uniform over the film's surface and is observed to decrease at the edges. Coherence is observed in the DRF over scales $|x_1 - x_2| < 0.05$, and so overall the response of absorber is partially-coherent. This coherence results from the ability of the induced current at one point to effect the current at a second point via the scattered field.

D. Choosing Z_S to maximise the absorbed power

When designing a resistive film TES detector, the surface impedance of the film is usually chosen to maximise the absorbed power. For electrically large ($p >> \lambda$) free-standing absorbers, it is usually assumed that the optimal value for Z_S is $0.5Z_0$ as a result of the analysis of the case of an infinite film (section III-C). However, there is no corresponding result or advice for electrically small films. In order to rectify this, we investigated the effect of Z_S on $\alpha = A_E(\theta = 0°)/p^2$ for various size films and the results are shown in figure 6. For each size of film, the effective area has been normalised to the film's physical area so that the curves can all be shown on the same axes. Also included is the analytic result for an infinite film, and it is reassuring the simulations tend to this line when $\frac{p}{\lambda}$ is large. As $\frac{p}{\lambda}$ decreases the curve are observed to become increasingly sharply peaked, and the location of the maxima to move. There appears to be no definite rule about the value of Z_S needed to match the film to free space. In the range $\frac{p}{\lambda} = 4.0 - 0.5$, the value of Z_S at which α is maximised –i.e. the match value– is observed to decrease with decreasing p. However, by $\frac{p}{\lambda} = 0.25$ it seems to have increased again. Consequently, these curves demonstrate that for optically small devices, full electromagnetic simulations, of the type described, will most likely be needed at the design stage to find the optimum Z_S.

The code also allows us to investigate the effect that a non uniform surface impedance has on the devices optical behaviour. In particular, we have studied the effect of 'striping' the film, i.e. breaking into up into an array of parallel strips, as opposed to one continuous film. Figure 7 shows A_E as a function of θ for two $\lambda \times \lambda$ films made out of the same material with the same $Z_S = 30\Omega$ (well below the match point). The film in 7(a) is continuous, while the film in (b) has been patterned into an array three identical strips in the y-direction, separated by two gaps of the same width and occupying the same overall footprint. The striping is seen to direct the films response to p-polarised waves forward: $A_E(0°)$ is increased and $A_E(90°)$ decreased compared with (a). The trade-off is that response to s-polarised waves is strongly suppressed in (b) compared with (a), which depending on the situation this may

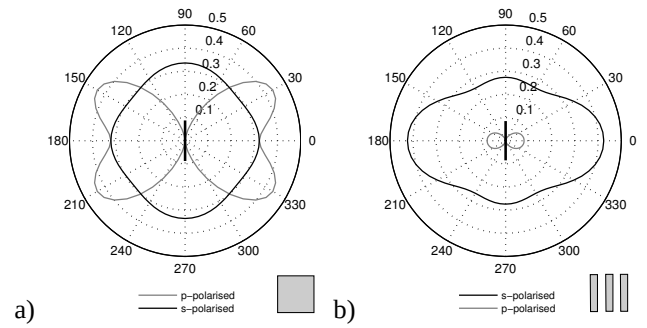

Fig. 7. Effect of striping the resistive film. Sub-figure (a) shows the results for a uniform $\lambda \times \lambda$ film with $Z_S = 30\Omega$. Sub-figure (b) shows results for identically sized film with the same Z_S, however the metallization has now been divided into three identical strips separated by gaps of equal width. The patterning of the film is shown in the bottom right-hand corner of each sub-figure.

or may not be beneficial. This behaviour can be explained in terms of the effective surface impedance of the striped film. To currents flowing parallel to the strip orientation, the film sections appear like a parallel array of lumped resistors. Adding more high resistance gaps will therefore push the effective film impedance in this direction up. For a low surface impedance material (e.g. 30Ω/sqr) this can bring the film's effective surface impedance closer to the match value. It is this effect that causes the increase in $A_E(0^\circ)$ for the s-polarised wave in 7(a). Currents attempting to flow perpendicular to the strips see a broken path and correspondingly a very high Z_S. This leads to the decrease in $A_E(90^\circ)$ for the p-polarised wave in 7(a). Striping offers the possibility of making resistive film detectors with highly polarised beams, or alternately a method of improving the matching of low Z_S films to free space.

V. Conclusions

It is possible to analyse the optical behaviour of certain classes of power detector in a rigorous way by using a method-of-moments like formulation to determine the power dissipated in the thin, resistive, films that comprise them. The far-field response, polarisation and natural detector can be calculated numerically, as well as the cross-talk between adjacent detectors in an array. To demonstrate the technique, full simulations of a single, isolated, resistive film TES detector were performed. The effect of the absorbing film's dimension and surface impedance have on the device's optical behaviour have been investigated rigorously, leading to the following recommendations:

- When the resistive film is electrically large and/or $Z_S >> Z_0$, the optical behaviour of the TES is well described by the simple model described in section III-C and [7]. When the absorbing film is electrically small and/or $Z_S < Z_0$, full electromagnetic simulations, as described here, must be performed to determine the value of Z_S required for a match, as well as other aspects of the optical behaviour.
- Resistive film bolometers are expected to be sensitive to stray light at high angles of incidence. This will not be so much of a problem in the centre of an imaging array, where the pixels shield each other. However it may be an issue for detectors at the edge. A possible solution is to introduce a guard ring around the array, which will also mitigate edge effects in the beams.
- By using a spatially varying surface impedance, the polarisation properties of the detector can be altered. A striped pattern can also be used to obtain a better match to free space when only low Z_S films can be fabricated. We have investigated the effect of 'striping' the film in detail, and hope to produce a paper with some design rules in the near future.

Future work will focus on analysing the interaction between the absorbing films in an imaging array. We have already determined how to include a ground plane in the simulations via the Green's dyadic. This will allow the analysis of a very common detector architecture, where a back-short is placed behind the film to improve absorption. Additionally, we are using the modelling scheme described in the paper as a tool in the development of a new class of end-fire absorber.

References

[1] S. Withington and G. Saklatvala, "Characterizing the behaviour of partially coherent detectors through spatio-temporal modes," *Journal of Optics A: Pure and Applied Optics*, vol. 9, pp. 626–633, 2007.

[2] S. Withington and C. Thomas, "Optical theory of partially coherent thin-film energy-absorbing structures for power detectors and imaging arrays," *Journal of the Optical Society of America A*, vol. 26, no. 6, pp. 1382–1392, 2009.

[3] T. Senior, "Backscattering from resistive strips," *IEEE Transactions on Antennas and Propagation*, vol. 27, pp. 808–813, 1979.

[4] M. Ney, "Method of moments as applied to electromagnetic problems," *IEEE Transactions on Microwave Theory and Techniques*, vol. 33, no. 10, pp. 972–980, 1985.

[5] S. Withington, M. Hobson, and R. Berry, "Representing the behavior of partially coherent optical systems by using overcomplete basis sets," *Journal of the Optical Society of America A*, vol. 21, no. 2, pp. 207–217, 2004.

[6] G. Saklatvala, S. Withington, and M. Hobson, "Coupled-mode theory for infrared and submillimeter wave detectors," *Journal of the Optical Society of America A*, vol. 24, no. 3, pp. 764–775, 2007.

[7] C. Thomas and S. Withington, "Modelling the intensity and polarisation response of planar bolometric detectors," *Accepted for publication in Journal of the Optical Society of America A.*

[8] S. Rao, D. Wilton, and A. Glisson, "Electromagnetic scattering by surfaces of arbitrary shape," *IEEE Transactions on Antennas and Propagation*, vol. 30, no. 3, pp. 409–418, 1982.

[9] X. Dardenne, "Method of moments simulation of infinite and finite periodic structures and application to high-gain metamaterial antennas," 2007.